Program Digest, 2019 IEEE International Ultrasonics Symposium (IUS)
Glasgow, Scotland, October 6-9, 2019

Visualization of a simulated lymph channel using contrast enhanced active Doppler ultrasonography method

1st Katsuya Saito
Graduate School of Science and Engineering
Chiba University, Chiba, Japan
skatsuya@chiba-u.jp

2nd Kenji Yoshida
Center for Frontier Medical Enginnering
Chiba University, Chiba, Japan
kenyoshi1980@chiba-u.jp

3rd Masaaki Omura
Graduate School of Science and Engineering
Chiba University, Chiba, Japan
m.omura@chiba-u.jp

4th Takuma Oguri
Ultrasound General Imaging
GE Healthcare, Tokyo, Japan
Graduate School of Sci. and Eng.
Chiba University, Chiba, Japan

5th Naohisa Kamiyama
Ultrasound General Imaging
GE Healthcare
Tokyo, Japan

6th Tadashi Yamaguchi
Center for Frontier Medical Enginnering
Chiba University, Chiba, Japan
yamaguchi@faculty.chiba-u.jp

Abstract— **This study proposed a method for visualizing lymph channels filled with stationary fluid, named contrast-enhanced active Doppler ultrasonography (CEADUS). CEADUS is quantified the translation of ultrasound contrast agent (UCA) due to the acoustic radiation force by Doppler method. In this report, we attempted to visualize a cylindrical channels with a diameter of 0.28 and 0.1-mm filled with a suspension of Sonazoid™ as UCAs in a tissue mimicking phantom containing acoustic scatterers. The single element concave transducer with 14.4-MHz center frequency was scanned at the step of 10 μm in the lateral direction, and ultrasound was emitted with pulse repetition frequency of 2 kHz at each scan line. We obtained two-dimensional images using dynamic information of the UCAs by analyzing for several seconds exposure duration in echo signals at each scanning line. As a result, the CEADUS image could be detected with high sensitivity even when the channel diameter was below the resolution.**

Keywords—Doppler effects, ultrasound contrast agent, acoustic radiation force, translational velocity, simulated lymph channel

I. INTRODUCTION

Techniques for visualizing the lymph channels can be applied in both diagnostic and therapeutic applications, such as intraoperatively identification of sentinel lymph nodes and lymphatic function evaluation in the diagnosis of lymphedema. The blue dye and lymphatic scintigraphy methods have been used in clinical to visualize lymph channels. On the other hand, near-infrared (NIR) fluorescence imaging has been interest in recent years because it has excellent real-time property and wide field of view without incisions. However, it cannot visualize lymph channels located at approximately 10 mm from the surface of tissue due to light scattering and absorption caused by passing through tissue [1]. We attempt to overcome this defect in NIR fluorescence imaging by combining with ultrasonography with good penetration depth.

Our *in-vivo* porcine experiments demonstrated that the visibility of lymph channels in conventional contrast-enhanced ultrasonography was sometime very poor depending on the situation. To increase the visibility, we have proposed a method for detecting the translation of ultrasound contrast agents (UCAs) caused by acoustic radiation force using the Doppler method, named contrast-enhanced active Doppler ultrasonography (CEADUS). We assume that the UCAs is injected subcutaneously into the skin tissue and absorbed into the lymph channels with stationary fluid or very slow flow, and additionally assumed that the UCAs float and stay on the top wall of the channel or they are dispersed throughout the channels. In such situation, it is expected that the acoustic radiation force moves the UCAs away from the transducer under ultrasound exposure. Dayton et al. showed that Albunex in a channel was displaced by 100 μm under 5-MHz ultrasonic radiation with a PRF of 1-10 kHz [2]. Tortoli et al. demonstrated that it was quantifiable by investigating the translational velocity of UCAs calculated by numerical simulation and measurement [3-6].

In order to visualize the lymph channels with a diameter of several tens or hundreds micron in subcutaneous tissue, we need to use ultrasound with a center frequency of 10-20 MHz and several cycles from the standpoint of resolution. In the case of a general UCA microbubbles with a resonance frequency of 3-5MHz [7,8], the translational velocity of UCAs should be slow under the exposure of 10-20 MHz ultrasound due to the mismatch with their resonance frequency. Although our previous phantom study has shown that the UCA translation could be quantified in the situation without clutter echo [9], we have not investigated the visibility of the simulated lymph channel in CEADUS method. In this report, we visualize a cylindrical channel with diameter same as typical lymph channels using the CEADUS method. The effectiveness of the CEADUS method was verified by comparing the contrast to noise ratio (CNR) as an index for the visibility.

II. Materials and Methods

A. Measurement target

To mimic scattering and attenuation characteristics of skin tissue, an agar phantom containing polyamide microspheres with a diameter of 10 μm (ORGASOL, Arkema) at 5wt% of scatterer concentration. Cylindrical channels with a diameter of 0.1, 0.28 mm were formed in the phantom. The channel was filled with a suspension of Sonazoid™ as UCAs with number density of 2.26×10^{12} bubbles/m^3.

B. Data acquisition

A single element concave transducer (V328, Olympus) with center frequency of 14.4 MHz and a focal length of 19.3 mm was located above from the channel for adjusting the focus to the center of the channel. Using a pulsar-receiver (Model 5800, Olympus), the transducer was excited at a pulse repetition frequency (PRF) of 2 kHz, and RF echo signals were acquired with an oscilloscope (HDO6104, LeCroy). The sampling frequency and the quantization rate was 250 MHz and 12 bits, respectively. The transducer was scanned at the step of 10 μm in the lateral direction, and the sequence of RF echo signals for 3 seconds were acquired at each scan line. The point spread function (PSF) of an ultrasonic beam was 79×208 μm (depth×lateral direction) and the condition for peak value of the negative sound pressure was 3.0 MPa, and the corresponding mechanical index (MI) was 0.79. In case of Sonazoid™ UCAs, it was reported that the UCAs began to collapse at MI = 0.4, and much of UCAs collapsed when MI > 1.0 [10].

C. Signal processing

1) Quantification of translational velocity of UCAs: The RF echo signals were repeatedly received at 1/PRF intervals and the RF signals per 1/PRF were rearranged in t-τ space as shown in Fig. 1, where t and τ meant the time corresponded to the depth and the pulse repetition time, respectively. Then the signal in t axis were converted to the analytical signal by Hilbert transform. We defined the change of the analytical signals in τ axis as Doppler signal. The frequency spectrum $S(t,f)$ and the power spectrum $P(t,f)$ of Doppler signal were obtained by applying the Fourier transform. Figure 2 shows typical examples of the power spectrum $P(t_0,f)$ of the Doppler signal at the depth corresponding to the center of the channel ($t = t_0$). Positive (negative) frequency components represent the translation moving away from (toward) the transducer. The expected value of the normalized power spectrum P_n of the Doppler signals were determined as Doppler shift frequency Δf as

$$\Delta f(t) = \int_{-f_{th}}^{f_{th}} f \cdot P_n(t,f)df, \tag{1}$$

$$P_n(t,f) = \frac{P(t,f)}{\int P(t,f)df}, \tag{2}$$

where f_{th} are integration interval and set to 50 Hz in order to reduce the noise effect in higher frequency range. Assuming that the UCAs moves on the sound propagation axis, we transformed the Δf into the velocity V_{UCA},

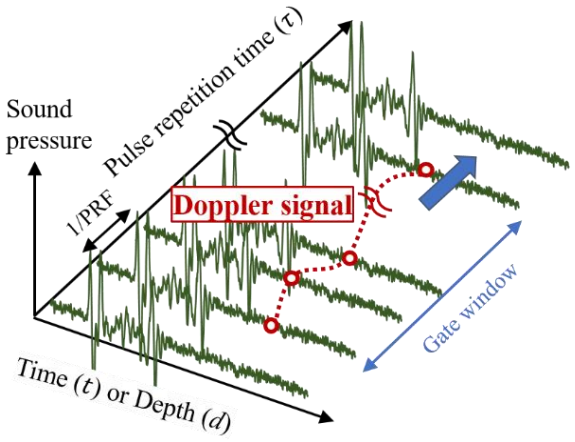

Fig. 1 Concept of Doppler signal.

$$V_{UCA} = \frac{\Delta f}{2f_0+\Delta f}c, \tag{3}$$

where f_0 and c are the center frequency of incident ultrasound and the speed of sound in surrounding media, respectively.

Assuming that the phantom around the channel was completely stationary, we defined the intensity of the Doppler signal of the UCAs, I_{dyn}, and the clutter signal, I_{sta}.

$$I_{sta}(t) = S(t,0), \tag{4}$$

$$I_{dyn}(t) = \int S(t,f)df - I_{sta}(t). \tag{5}$$

Two-dimensional images of I_{sta}, I_{dyn} and V_{UCA} were generated by applying the above process to all scan lines.

2) Analysis of time-change in parameters: I_{sta}, I_{dyn} and V_{UCA} were calculated at a given time (depth) based on the analysis of Doppler signal for several seconds exposure duration. The time change of these parameters were evaluated by delaying the analyzed gate window along the τ axis with step of 0.5 μs (Fig. 1). The length of gate window were 0.4 seconds for a 0.28 mm channel and 0.3 seconds for a 0.1 mm channel.

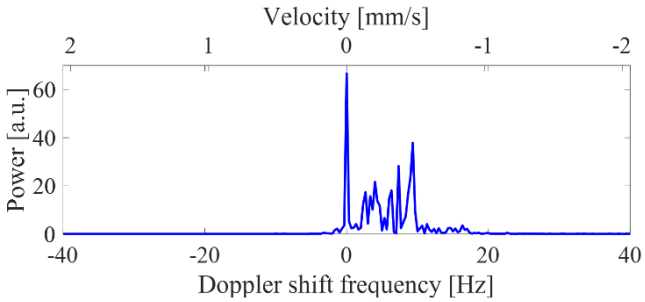

Fig. 2 Typical power spectrum of Doppler signal.

III. Results

1) Visualizing of a simulated channel: Figure 3 and 4 show the images of the channel with a 0.28 and 0.1 mm diameter in the phantom. In both figures, (a) show B-mode images of the echo intensity distribution from single transmission/reception data in each scanning line. (b)-(d) show the two-dimensional disutribution images of the intensity of the stationary echo component I_{sta} the dynamic echo component I_{dyn}, the translational velocity of UCAs V_{UCA} Each image is normalized by its maximum value in the field of view, and the image after logarithmic compression is displayed with a dynamic range of 40 dB (i.e. the velocity range is 0.01-1 mm/s in case of V_{UCA}). In both figures, although the channels were indistinguishable in B-mode image, the locations of channels were detectable with high contrast in the images of I_{dyn} and V_{UCA}. In case of the channel with a 0.28 mm, the channel could be extracted nearly as a circle. On the other hand, the shape of 0.1 mm channel was obscure. However, we should emphysize that it could be detected sufficiently even though the size of channel was less than the lateral resolution.

We evaluated contrast-echo to noise-echo ratio (CNR) between the channel and surrounding phantom in order to discuss the visibility of the channel quantitatively.

$$CNR(\tau) = \frac{|\mu_{UCA}(\tau) - \mu_{clutter}(\tau)|}{\sqrt{\sigma_{UCA}(\tau) + \sigma_{clutter}(\tau)}}, \quad (6)$$

where μ and σ are the mean and dispersion of the evaluation index in region of interest (ROI). The channel position was identified based on the B-mode image when the channel was filled with phosphate buffered saline. A circle with a diameter of 0.28 mm was set as the ROI at the center of the channel, and the inside of the circle was defined as the chamber area and the outside was as the surrounding phantom area. Each CNR in the images shown in Fig. 3(a)-(d) was calculated as 0.60, 0.08, 1.91, 2.28, respectively. It was confirmed CNR is improved by 20 times or more compared to the conventional method (Fig. 3(a)) by using the dynamic information of UCAs as shown in Fig. 3(c) and (d). In case of 0.1 mm channel diameter, it was smaller than the resolution. Therefore, the size of the portion with relatively higher value for I_{dyn} and V_{UCA} was larger than the real size of the channel (0.1 mm) as shown in Fig.4 (c) and (c), leading to the increasing of $\mu_{clutter}$ and $\sigma_{clutter}$ in Eq. (6). As a result, we could not accurately analyze the CNR.

2) Time-change in CNR: It is necessary to verify whether the translation of UCAs can be detected continuously and discuss the practical utility of CEADUS. Figure 5 shows the time-change in CNR for each evaluation index. CNR for especially I_{dyn} and V_{UCA} exponentially decreased. Therefore we conducted the fitting of CNR-τ curve by using the following equation and obtained the parameters A, B and time constant T_c:

$$CNR_{fit}(\tau) = A + B\exp(-\tau/T_c). \quad (7)$$

In Table I, the parameters A, B, T_c and determination coefficient R^2 for each curve are summarized. Because the determination coefficient R^2 was very small in case of I_{sta}, the resultant parameters for I_{sta} were excluded in this table. CNR relating to dynamic information of UCAs i.e. I_{dyn} and V_{UCA} kept to be higher than 1 during ultrasound exposure although they exponentially decreased with time constant of approximately 0.5-1 s. On the other hand, the CNR of conventional B mode was always lower than 0.5 although its time constant was smaller than that of I_{dyn} and V_{UCA}. Although we speculate that the decrease in CNR results from the restriction of UCA translation possibly influenced by the relationship the travel distance of UCAs and the channel diameter [9], it will be investigated in the future.

TABLE I. PARAMETERS A, B AND T_c AND R^2 FOR CNR-T CURVES

	A	B	T_c (s)	R^2
B-mode	0.153	0.35	1.67	0.27
I_{dyn}	1.26	0.80	0.45	0.62
V_{UCA}	1.36	0.60	0.89	0.74

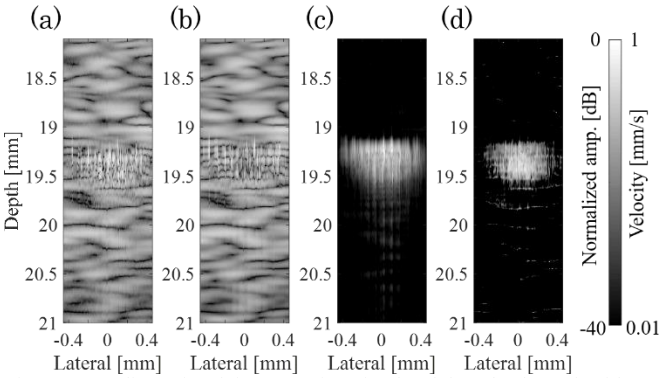

Fig. 3 Two dimensional images of a simulated lymph channel with a diameter of 0.28 mm using (a) B-mode image, (b) stationary component, (c) dynamic component, (d) translational velocity of UCAs.

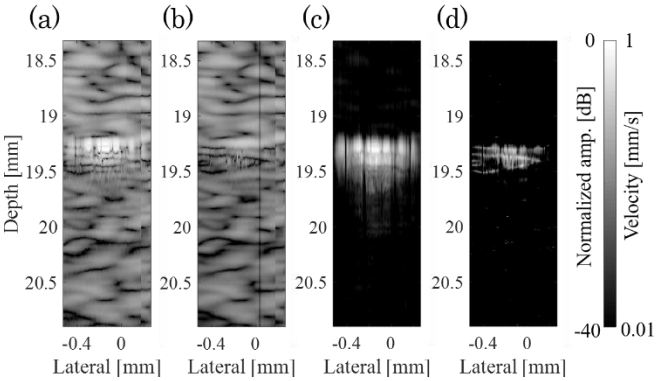

Fig. 4 Two dimensional images of a simulated lymph channel with a diameter of 0.1 mm using (a) B-mode image, (b) stationary component, (c) dynamic component, (d) translational velocity of UCAs.

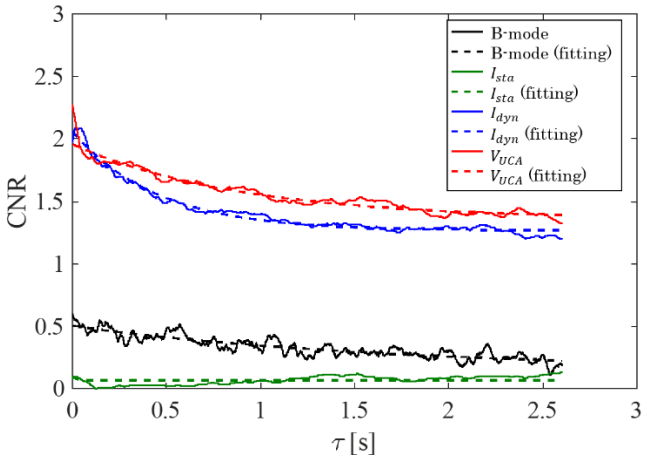

Fig. 5 Change in CNR over time for each evaluation index and time constant calculated after fitting using Eq.(7).

IV. Discussion

To realize the CEADUS as effective method in clinical situation, it is required to improve detection accuracy of lymph channels and real time property. For the former, we must overcome the effect of clutter echoes due to such as arterial pulsation. For example, peripheral vessel wall of an artery has a velocity of up to 10 mm/s [11]. Although the pulsation of capitally is assumed to be slower than this value, we consider that the translational velocity of UCAs is required faster than 1 mm/s at least. Because we could not induce the translational velocity faster than 1 mm/s, the ultrasound transmitting condition for e.g. PRF and sound pressure should be optimized.

Furthermore, the UCA translational velocity should be faster from the standpoint of the real-time property in CEADUS. As abovementioned, the UCA translational velocity was slower than 1 mm/s in current ultrasound transmitting condition. To accurately evaluate the velocity and keep the better CNR, therefore, we need to continue the ultrasound transmitting for several hundred mili-seconds per each scan line for enhancing the UCA translation. As a result, it takes a long time to make a one frame image by scanning the ultrasound beam, leading to much poor frame rate. We believe that this problem can be improved by high frame rate (HFR) imaging using plane wave [12], where all UCAs in the field of view were simultaneously driven with high pulse repetition frequency. It would be a better way to increase the translational velocity of UCAs so that increasing the PRF rather than the sound pressure can prevent the collapsing of UCAs. Thus, HFR imaging using plane wave may solve both problems for motion artifact and real-time property. In the future, we will construct this HFR imaging system with plane wave and improve detection sensitivity of CEADUS method.

V. Conclusion

In this report, we attempted to visualize a simulated lymph channel using CEADUS, which quantifies the slight change of UCAs caused by acoustic radiation force. Although it was difficult to identify a simulated lymph channel from B-mode images, it was shown that high contrast images could be obtained by imaging change of UCA generated during ultrasound irradiation period. It was also implied that a simulated lymph channel can be detected with high sensitivity even if the channel diameter is less than the resolution.

Acknowledgment

This work was partly supported by Terumo Foundation for Life Sciences and Arts, and JSPS Core-to-Core Program, KAKENHI Grant Numbers 19H04436, 17K11529, and the Institute for Global Prominent Research at Chiba University.

References

[1] J.T. Alander, I. Kaatinen, A. Laakso, T. Spillmann, V.V. Tuchin, M. Venermo and P. V Spillmann, VV. Tuchin, M. Venermo and P. Välisuo, “A review of indocyanine green fluorescent imaging in surgery,” J. Biomed. Imaging, vol. 7, January 2012.

[2] P.A. Dayton, K.E. Morgan, A.L. Klibanov, G. Brandenburger, K.R. Nightingale and K.W. Ferrara, “A Preliminary evaluation of the effects of primary and secondary radiation forces on acoustic contrast agents,” IEEE Trans. Ultrason. Ferroelectr. Freq. Conrol, vol. 44, no. 6, pp. 1264-1277, November 1997.

[3] P. Tortoli, D. Bagnai and D. Righi, “Quantitative analysis of Doppler spectrum modifications yielded by contrast agents insonified at high pressure,” IEEE Trans. Ultrason. Ferroelectr. Freq. Control, vol. 46, no. 1, pp. 247–251, 1999.

[4] P. Tortoli, E. Boni, M. Corsi, M. Arditi and P. Frinking, “Different effects of microbubble destruction and translation in Doppler measurements,” IEEE Trans. Ultrason. Ferroelectr. Freq. Control, vol. 52, no. 7, pp. 1183–1188, 2005.

[5] P. Tortoli, F. Guidi, R. Mori and H.J. Vos, ”The use of microbubbles in Doppler ultrasound studies,” Med. Biol. Eng. Comput., vol. 47, no. 8, pp. 827-838, August 2009.

[6] H.J. Vos, F. Guidi, E. Boni and P. Tortoli, “Method for microbubble characterization using primary radiation force,” IEEE Trans. Ultrason. Ferroelectr. Freq. Control, vol. 54, no. 7, pp. 1333–1344, 2007.

[7] K. Yoshida, K. Tamura and T. Yamaguchi, “Estimation of size and number density of microbubbles based on analysis of frequency-dependent attenuation,” Jpn. J. Appl. Phys, vol. 55, no. 7, 07KC03-8, 2016.

[8] K. Sarkar, W.T. Shi, D. Chatterjee and F. Forsberg, “Characterization of ultrasound contrast microbubbles using in vitro experiments and viscous and viscoelastic interface models for encapsulation,” J. Acoust. Soc. Am., vol. 118, no. 1, pp. 539-550, 2005.

[9] K. Yoshida, K. Saito, M. Omura, K. Tamura and T. Yamaguchi, “Ultrasound assessment of contrast-agent motion driven by acoustic radiation force in a channel filled with stationary fluid,” J. Acoust. Soc. Am. (accepted).

[10] W.T. Shi, F. Forsberg, A. Tornes, J. Østensen and B.B. Goldberg, “Destruction of contrast microbubbles and the association with inertial cavitation,” Ultrasound in Med. Biol., vol. 26, no. 6, pp. 1009-1019, 2000.

[11] R. Nagaoka, G. Masuno, K. Kobayashi, S. Yoshizawa, S. Umemura and Y. Saijo, “Measument of regional pulse-wave velocity using spatial compound imaging of the common carotid artery in vivo,” Ultrasonics, vol. 55, pp. 92-103, 2015.

[12] L.M. Blue, F. Guidi, H.J. Vos, C.J. Slagle, M.A. Borden and P. Tortoli, “Plane wave contrast imaging: a radiation force point of view,” IEEE Trans. Ultrason. 9 Ferroelectr. Freq. Control, vol. 65, no. 12, 2018.